A solid state NMR and X-ray crystallographic investigation of dynamic disorder in solid tetrahydronaphthalene derivatives

Glenn A. Facey, Terrence J. Connolly, Corinne Bensimon, and Tony Durst

Abstract: The solid state disorder of two tetrahydronaphthalene derivatives, *N*-methyl-*N*-methoxy-5,6,7,8-tetrahydro-1-naphthamide and 5,6,7,8-tetrahydro-1-naphthoic acid, was studied by solid state NMR and single crystal X-ray diffraction. The X-ray crystal structure of *N*-methyl-*N*-methoxy-5,6,7,8-tetrahydro-1-naphthamide was obtained at 123 K. It indicated the presence of two distinct molecular conformations. Solid state ^{13}C CP/MAS NMR data using the dipolar dephasing technique revealed that the two conformations of the molecule are dynamically disordered, while solid state ^{2}H NMR data, collected on a specifically deuterated analog, were used to determine the populations of each conformation as well as an apparent activation energy. Solid state NMR experiments were also used to show that 5,6,7,8-tetrahydro-1-naphthoic acid possesses the same type of dynamic disorder.

Key words: deuterium NMR, solid state NMR, dynamic disorder, X-ray, tetrahydronaphthalene derivatives

Résumé : Faisant appel à la RMN à l'état solide et à la diffraction des rayons X sur un cristal unique, on a étudié le désordre à l'état solide de deux dérivés du tétrahydronaphthalène, le *N*-méthyl-*N*-méthoxy-5,6,7,8-tétrahydro-1-naphthamide et de l'acide 5,6,7,8-tétrahydro-1-naphthoïque. On a déterminé la structure cristalline du *N*-méthyl-*N*-méthoxy-5,6,7,8-tétrahydro-1-naphthamide à 123 K. Elle indique la présence de deux conformations moléculaires distinctes. Les données de la RMN CP/MAS du ^{13}C à l'état solide, obtenues en utilisant la technique du déphasage dipolaire, ont révélé que les deux conformations de la molécule sont dynamiquement désordonnées; on a utilisé les données de la RMN du ^{2}H à l'état solide, obtenues à l'aide d'un analogue spécifiquement deutéré, pour déterminer les populations de chacun des conformères ainsi qu'une énergie d'activation apparente. On a aussi utilisé les expériences de RMN à l'état solide pour montrer que l'acide 5,6,7,8-tétrahydro-1-naphtoïque présente le même type de désordre dynamique.

Mots clés : RMN du deutérium, RMN à l'état solide, désordre dynamique, rayons X, dérivés tétrahydronaphtalènes.

[Traduit par la rédaction]

Introduction

The structural characterization of molecules is typically tackled with a broad arsenal of techniques including all forms of spectroscopy, mass spectrometry, and diffraction. Often chemists will put a great deal of effort into the growth of single crystals suitable for X-ray diffraction analysis, as this technique is often the one that will prove, beyond doubt, the structure of the material in question. In this contribution, we would like to illustrate that although often essential, single crystal X-ray diffraction data can be open to interpretation and that in such instances solid state NMR spectroscopy is an essential complementary technique needed to fully characterize the solid state structure. Single crystal X-ray diffraction is a technique sensitive to long-range order. The collection of data takes hours or days. These two facts render the technique unable to distinguish between static disorder and dynamic disorder.

Unlike single crystal diffraction techniques, solid state NMR spectroscopy is a technique sensitive to short-range order. Typical data collection times for a single transient are on the hundreds of microseconds to tens of milliseconds time scale. These two facts make this technique sensitive to molecular motions and, as a result, the distinction between static and dynamic disorder is possible. Also, it has the advantage that polycrystalline powders rather than single crystals can be used. This study involves the structural characterization of the two tetrahydronaphthalene derivatives **5a** and **6a** (Scheme 1). It demonstrates the complementary nature of single crystal X-ray diffraction and solid state NMR spectroscopy.

Background

^{2}H is a spin $I = 1$ nucleus having three Zeeman states. The pure Zeeman states are perturbed by the electric quadrupolar interaction, producing two resonance frequencies for each crystallographically unique deuteron. The difference in frequency between the two resonances is determined by the quadrupolar coupling constant, $\chi = (e^2Qq//h)$, and the orientation of the electric field gradient tensor at the nuclear site with respect to the static magnetic field. For deuterons

Received June 18, 1996.

G.A. Facey,[1] T.J. Connolly, C. Bensimon, and T. Durst. Department of Chemistry, University of Ottawa, Ottawa, ON K1N 6N5, Canada.

[1] Author to whom all correspondence may be addressed. Telephone: (613) 562-5800, ext. 6077. Fax: (613) 562-5170. E-mail: gafacey@oreo.chem.uottawa.ca

Scheme 1. Reagents: (a) K_2CO_3, THF:D_2O, Δ; (b) $LiAlH_4$, THF; (c) (*i*) *n*BuLi, TMEDA, Pentane, Δ, (*ii*) CO_2(s), (*iii*) HCl; (d) H_2, Pd/C, HOAc; (e) (*i*) $SOCl_2$, CH_2Cl_2, Δ, (*ii*) $(MeO(Me)NH_2^+Cl^-$, Et_3N, CH_2Cl_2.

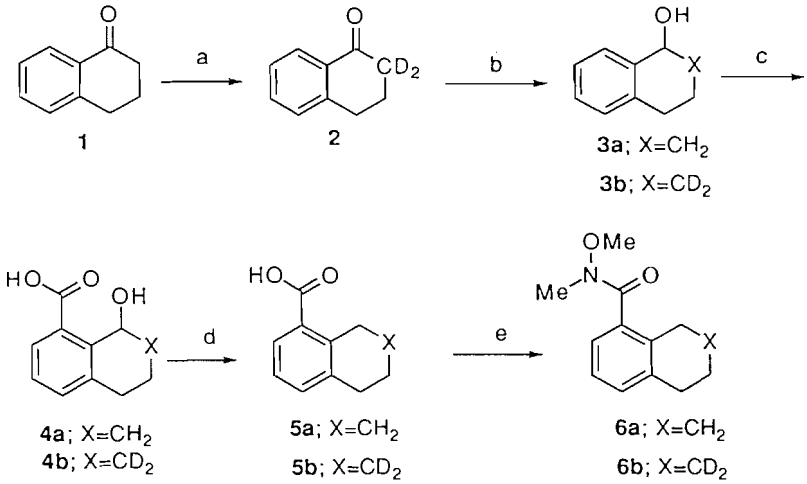

attached to carbon atoms the electric field gradient tensor, V_{ij}, is very often axially symmetric with its largest component, $V_{zz} = eq$, parallel to the C—D bond and, since V_{ij} has a trace of zero, $V_{zz} = (V_{yy} + V_{xx})$ with $V_{yy} = V_{xx}$. In the cases where axial symmetry is not present, it is conventional to assign $V_{zz} > V_{yy} > V_{xx}$. It is useful to define an asymmetry parameter, η, where $\eta = (V_{yy} - V_{xx})/V_{zz}$ where $0 \leq \eta \leq 1$.

The ^2H NMR spectrum of a single crystal consists of a sharp doublet for every crystallographically distinct deuteron whose splitting depends on the orientation of the crystal with respect to the magnetic field. For polycrystalline powders, where all orientations of the crystals are represented equally, the result is an envelope or powder spectrum from the sum of all possible doublets. The lineshape for such spectra can be readily calculated (1). In general, the spectra are symmetric about the centre with three pairs of singularities separated by frequencies, $\Delta\nu_{zz}$, $\Delta\nu_{yy}$, and $\Delta\nu_{xx}$, where $\Delta\nu_{zz} > \Delta\nu_{yy} > \Delta\nu_{xx}$. The frequency separations are proportional to the principal components of V_{ij} and are given by:

$$[1] \qquad -\Delta\nu_{XX} = \frac{-3\chi}{4}(1-\eta)$$

$$[2] \qquad -\Delta\nu_{YY} = \frac{-3\chi}{4}(1+\eta)$$

$$[3] \qquad \Delta\nu_{ZZ} = \frac{3\chi}{2}$$

The negative signs are added to the frequency differences to maintain a trace of zero.

The electric quadrupolar interaction, dominating the lineshapes of solid state ^2H NMR spectra, is exceedingly sensitive to molecular motions (2). The motions give rise to an averaged electric field gradient tensor and modify the shape of the powder spectrum. The effects can be grouped into three categories based on the rates of the molecular motion:

(a) Slow motions: These are motions occurring on a time scale much longer than the reciprocal line width of the static spectrum ($\sim 10^4$ s^{-1}). The effects are negligible on the NMR spectrum as there is essentially no change in the electric field gradient tensor during the course of the quadrupolar echo measurement.

(b) Intermediate rate motions: These are motions that occur on a time scale of the same order as the reciprocal line width of the static spectrum ($\sim 10^4$–10^7 s^{-1}). These motions have a profound effect on the observed lineshape (3–6). The lineshapes are very sensitive to the spacing between the pulses in the quadrupolar echo experiment (7) as well as to the rate and mechanism of the molecular motion. Although reduced significantly in amplitude compared to the rigid spectrum, the intermediate rate spectra can be simulated (8–10) in order to confirm a particular mechanism of a molecular motion or to determine its rate at the temperature of the measurement.

(c) Fast molecular motions: These motions occur on a time scale much shorter than the reciprocal line width of the static spectrum ($>10^7$ s^{-1}). The motion gives rise to an averaged electric field gradient tensor and spectra take on the same type of lineshape as those for rigid systems with the frequency differences between pairs of spectral singularities reduced. Such spectra are insensitive to the rate of the motion but may often be used to confirm the mechanism for the molecular motion. Fast motion limit spectra may be temperature dependent in cases where the population ratio for the sites occupied during the motion changes with temperature (11).

Experimental

All solid state NMR spectra were acquired on a Bruker ASX-200 solid state NMR spectrometer. Solid state ^{13}C CP/MAS spectra were acquired using a Bruker MAS probe with 7 mm o.d. zirconia rotors. The ^1H π/2 pulses were 3.6 μs, and 1 ms contact times were used. The spinning rate was set at 4000 Hz and was stable to within 2 Hz. In some cases the spinning side bands were suppressed (12). The solid state ^2H NMR spectra were acquired using a Bruker wideline probe accepting 5 mm o.d. glass tubes. The quadrupolar echo tech-

nique (13) was used with 3.2 μs $\pi/2$ pulses and an interpulse delay of 35 μs. The receiver was gated on 33 μs after the second pulse and the data were left shifted to the top of the echo before Fourier transformation. Although the temperature was regulated with the variable temperature control unit of the spectrometer, it was measured directly by placing a thermocouple on the rf coil containing the sample immediately after data collection. The reported temperatures are accurate and precise to within 1 degree. ^2H T_1 measurements were made using the inversion–recovery technique with magnetization being sampled with a quadrupolar echo. In all measurements at least 10 recovery times were used and the T_1's were calculated using the three-parameter nonlinear fit provided by the software of the spectrometer.

The single crystal X-ray data for **6a** were collected at 123 K on a Rigaku diffractometer with Cu Kα radiation using the ω–2θ scan technique to a maximum 2θ value of 100°. The cell constants and an orientation matrix for data collection were obtained from least-squares refinement using the setting angles of 25 reflections in the range $80° < 2\theta < 100°$. A total of 1297 reflections was collected. The unique set contained only 1195 reflections. The standards were measured after every 150 reflections. No crystal decay was noticed. The data were corrected for Lorentz and polarization effects, no correction being made for absorption. The structure was solved by direct methods. All non-hydrogen atoms were refined anisotropically. The maximum and minimum peaks in the final difference Fourier map corresponded to 0.460 and −0.440 e/Å^3, respectively.

All materials used for this study were prepared according to Scheme 1 (14) and the details dealing with the synthesis will be published elsewhere.

Results and discussion

The single crystal X-ray diffraction data (deposited as supplementary material)[2] for **6a** taken at 123 K show that the compound crystallizes in the space group $P2_1/a$ with four molecules in the unit cell. The cell constants are as follows: a = 8.6171 Å; b = 12.2350 Å; c = 11.2223 Å, and β = 102.937°. An ORTEP plot of the structure is given in Fig. 1. The structure shows a molecular confirmation where the carbonyl bond is almost normal to the plane of the aromatic ring, thus leaving a great deal of void space around the methylene carbons in the 6 and 7 positions. Another very obvious feature of the crystal structure is that there are two sets of coordinates found for each of the carbons in the 6 and 7 positions of the cyclohexene moiety. This indicates that there are two conformations of the cyclohexene ring present in the crystal. The disorder was refined using fixed thermal parameters and letting the occupancies for the four sites occupied by carbons 6 and 7 refine. The results gave occupancies close to 0.75:0.25. The occupancies were then fixed to these values

Fig. 1. ORTEP plot of the crystal structure of **6a** at 123 K refined under the assumption that the population ratio is 0.75:0.25.

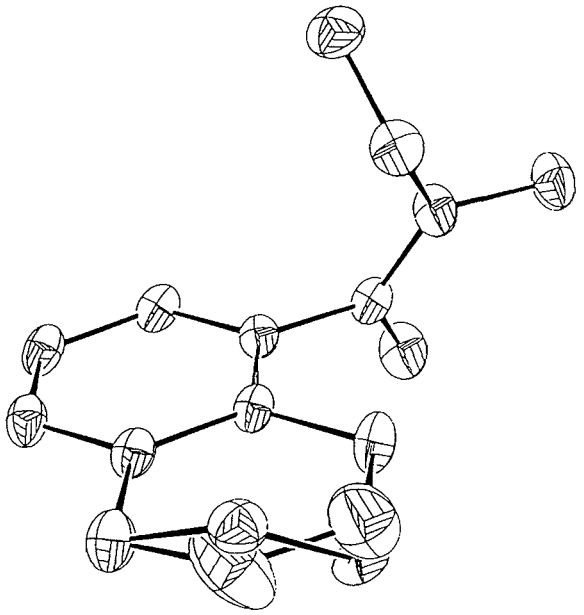

and the thermal parameters refined. It is interesting to note that the thermal parameters are not equal for each of the two conformations, the major conformation having much larger thermal parameters than the minor one. One possible explanation of this may be that the local intermolecular forces for each of the sites may be different, allowing one of the conformations to have slightly more mobility than the other. The X-ray data are unable to confirm whether the structure is rigid with both conformations present (static disorder) or whether the two conformations are exchanging dynamically with one another (dynamic disorder).

The solid state ^{13}C CP/MAS NMR spectrum of **6a** taken at room temperature is shown in Fig. 2*A*. The spectrum is highly resolved, each nonequivalent carbon giving rise to a resonance. The only coincidental overlap occurs for the resonances of the carbons in the 6 and 7 positions on the cyclohexene ring. The carbonyl carbon and the *N*-methyl carbon are broadened from partially unaveraged dipolar interactions between ^{13}C and ^{14}N (15). If there was a static disorder in the structure at room temperature, one might expect to observe two resonances for each carbon atom in the molecule, one set for each of the two nonequivalent conformations (16). Furthermore, the intensities of the lines would approximately represent the population ratio of the conformers present. This does not seem to be the case. The ^{13}C CP/MAS spectrum acquired with dipolar dephasing is given in Fig. 2*B*. In dipolar dephasing experiments (17) a short delay (40 μs in this case) is inserted between the contact pulse and the beginning of the acquisition. During this delay the $^{13}C - {}^1H$ dipolar interactions are only partially averaged by the magic angle spinning. Also, the magnetization due to carbon nuclei having large $^{13}C - {}^1H$ dipolar interactions dephases and the corresponding resonances are absent from the frequency domain spectrum. This is true for fairly rigid carbon atoms directly bound to protons. Carbon atoms not bearing protons or methyl car-

[2] Supplementary material can be purchased from: The Depository of Unpublished Data, Document Delivery, CISTI, National Research Council Canada, Ottawa, Canada K1A 0S2. These data have also been deposited with the Cambridge Crystallographic Data Centre, and can be obtained on request from The Director, Cambridge Crystallographic Data Centre, University Chemical Laboratory, 12 Union Road, Cambridge, CB2 1EZ, U.K.

Fig. 2. (*A*) ^{13}C CP/MAS NMR spectrum of **6a** at room temperature. (*B*) Same as *A* with a 40 μs dipolar dephasing delay. In both traces the first-order spinning side bands were suppressed (12).

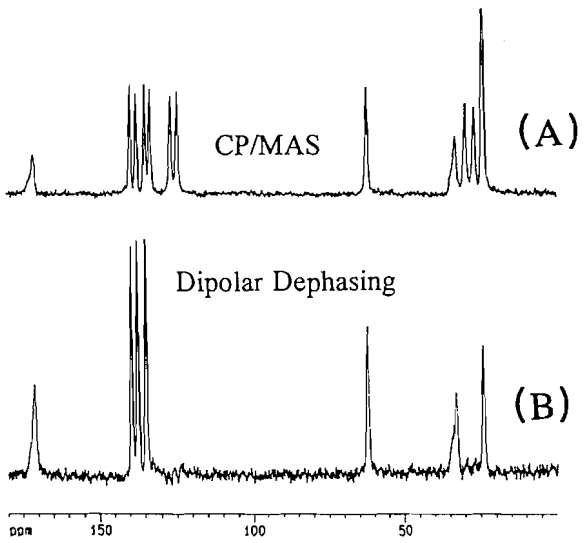

bons whose dipolar interactions with protons are averaged as a result of fast methyl group rotation, will show up in the spectrum, albeit slightly attenuated. The data in Fig. 2*B* show that not only do the carbonyl, methyl, and quaternary aromatic resonances survive the dephasing delay, but the 6 and 7 methylene carbons of the cyclohexene ring do as well. This can be the case only if the ^{13}C – ^{1}H dipolar interactions for these methylene carbons are averaged by some sort of molecular motion. Therefore, we can conclude that the nature of the disorder present in the structure at room temperature is dynamic rather than static. This, however, does not prove whether or not the disorder observed at 123 K in the X-ray data is static or dynamic in nature.

The analogue to **6a** labelled with deuterium on the 7 position, **6b**, was prepared to address the dynamic nature of the structural problem. The wideline solid state ^{2}H NMR spectra of **6b** are given in Fig. 3 as a function of temperature. At all temperatures the width of the powder spectrum is narrower than one would expect for a completely rigid system (18). Furthermore, at all temperatures above 178 K, the ^{2}H NMR spectra are in the fast motion limit. That is, the molecular motion is occurring at a rate much greater than the reciprocal width of the rigid powder spectrum (expected to be ~260 kHz) (18). Spectra collected below 178 K are in the intermediate motion regime. The separation between the spectral singularities at the top, middle, and base of the powder spectra are plotted against temperature in Fig. 4. One can see that one splitting (the separation of the middle shoulders) remains essentially constant throughout the entire temperature range. This indicates that the axis of the molecular motion must lie parallel to one of the two principal components of the electric field gradient tensor perpendicular to the C—D bond. Furthermore, the lineshape observed at 300 K is characteristic of a two-site exchange between equally populated sites with the C—D bond subtending the tetrahedral angle over the course of the motion. (18) These observations

Fig. 3. Broadline solid state ^{2}H NMR spectra of **6b** recorded as a function of temperature. The relaxation delay was greater than the T_1 by at least a factor of 5.

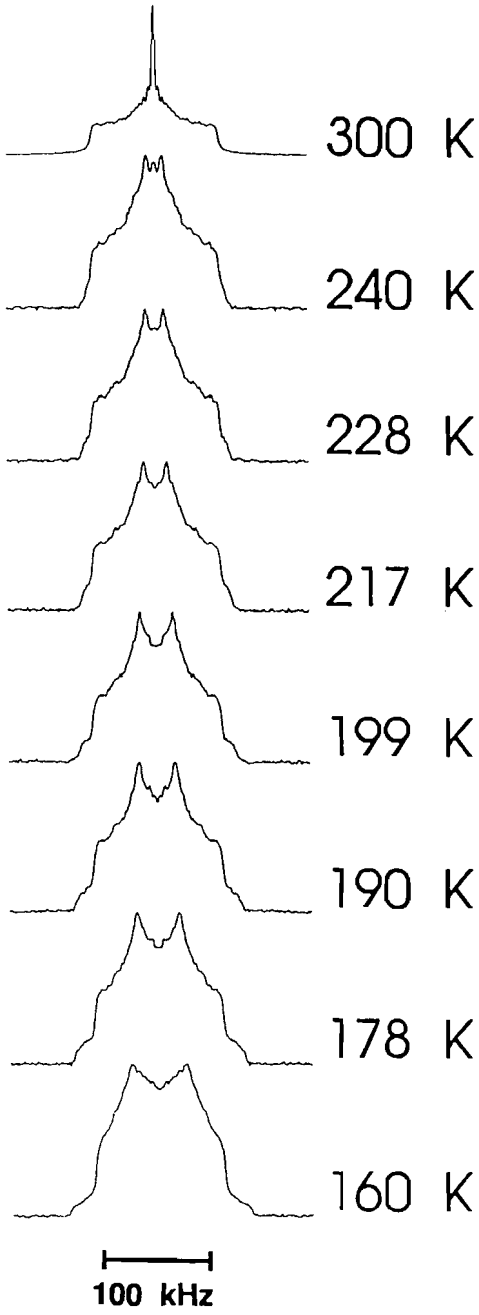

are consistent with the model depicted in figure 5. In this model, the cyclohexene moiety undergoes a transformation akin to the chair to chair inversion of cyclohexane. The sites however must not be equally populated over the entire temperature range as this would leave the spectra invariant with temperature. As the temperature is lowered one site becomes more populated than the other. The frequency differences between the singularities of the fast motion lineshape are determined by the eigenvalues of the averaged electric field gradient tensor. These are calculated by taking the weighted average of the electric field gradient tensors for each of the

Fig. 4. Plot of the frequency differences, $\Delta\nu'_{XX}$, $\Delta\nu'_{YY}$, and $\Delta\nu'_{ZZ}$, between the features of the solid state ^2H spectra of **6b** as a function of temperature.

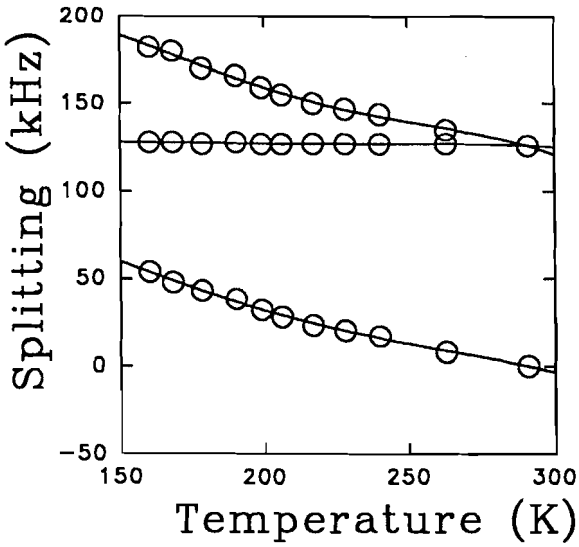

Fig. 5. Model depicting the inversion of the cyclohexene moiety.

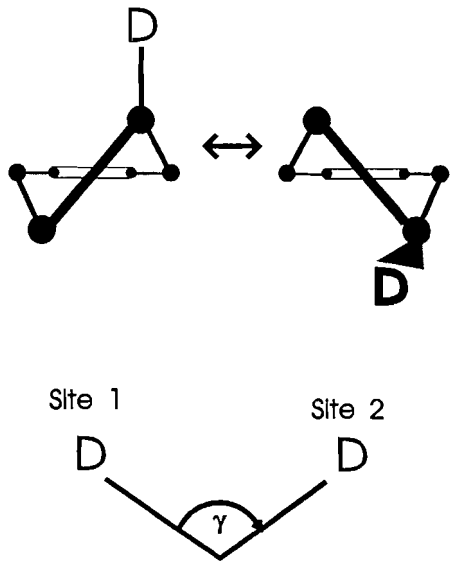

sites occupied over the course of the molecular motion, then diagonalizing the averaged tensor if necessary. To do this calculation we must define all of the electric field gradient tensors in a common axis system. This is most conveniently accomplished by choosing an axis defined by the motion and then redefining each of the tensors with respect to this new axis system in terms of the Euler angles, α, β, and γ (19). The electric field gradient for each of these sites is defined as follows:

$$[4] \qquad V(\alpha, \beta, \gamma) = \begin{bmatrix} a_{11} & a_{12} & a_{13} \\ a_{21} & a_{22} & a_{23} \\ a_{31} & a_{32} & a_{33} \end{bmatrix}$$

where $a_{ij} = a_{ji}$. Each of the matrix elements are defined as follows:

$$[5] \quad a_{11} = (\cos^2\alpha \cos^2\beta \cos^2\gamma + \sin^2\alpha \sin^2\gamma - 2 \sin\alpha \cos\alpha \cos\beta \sin\gamma \cos\gamma)V_{XX} + (\sin^2\alpha \cos^2\beta \cos^2\gamma + \cos^2\alpha \sin^2\gamma + 2\sin\alpha \cos\alpha \cos\beta \sin\gamma \cos\gamma)V_{YY} + (\sin^2\beta \cos^2\gamma)V_{ZZ}$$

$$[6] \quad a_{22} = (\cos^2\alpha \cos^2\beta \sin^2\gamma + \sin^2\alpha \cos^2\gamma + 2\sin\alpha \cos\alpha \cos\beta \sin\gamma \cos\gamma)V_{XX} + (\sin^2\alpha \cos^2\beta \sin^2\gamma + \cos^2\alpha \cos^2\gamma - 2\sin\alpha \cos\alpha \cos\beta \sin\gamma \cos\gamma)V_{YY} + (\sin^2\beta \sin^2\gamma)V_{ZZ}$$

$$[7] \quad a_{33} = (\cos^2\alpha \sin^2\beta)V_{XX} + (\sin^2\alpha \sin^2\beta)V_{YY} + (\cos^2\beta)V_{ZZ}$$

$$[8] \quad a_{12} = (-\cos^2\alpha \cos^2\beta \sin\gamma \cos\gamma + \sin^2\alpha \sin\gamma \cos\gamma + \sin\alpha \cos\alpha \cos\beta(\sin^2\gamma - \cos^2\gamma))V_{XX} + (-\sin^2\alpha \cos^2\beta \sin\gamma \cos\gamma + \cos^2\alpha \sin\gamma \cos\gamma + \sin\alpha \cos\alpha \cos\beta(\cos^2\gamma - \sin^2\gamma))V_{YY} + (-\sin^2\beta\cos\gamma \sin\gamma)V_{ZZ}$$

$$[9] \quad a_{13} = (\cos^2\alpha \cos\beta \sin\beta \cos\gamma - \sin\alpha \cos\alpha \sin\beta \sin\gamma)V_{XX} + (\sin^2\alpha \sin\beta \cos\beta \cos\gamma + \cos\alpha \sin\alpha \sin\beta \sin\gamma)V_{YY} + (-\sin\beta \cos\beta \cos\gamma)V_{ZZ}$$

$$[10] \quad a_{23} = (-\cos^2\alpha \cos\beta \sin\beta \sin\gamma - \sin\alpha \cos\alpha \sin\beta \cos\gamma)V_{XX} + (-\sin^2\alpha \sin\beta \cos\beta \sin\gamma + \sin\alpha \cos\alpha \sin\beta \cos\gamma)V_{YY} + (\sin\beta \cos\beta \sin\gamma)V_{ZZ}$$

For the two-site model described in Fig. 5, we can define an axis normal to the plane defined by the two-site exchange with the origin on the carbon atom and then define the Euler angles with respect to this axis. We have $\alpha_1 = 0°$, $\beta_1 = 90°$, and $\gamma_1 = -54.75°$ for one site and $\alpha_2 = 0°$, $\beta_2 = 90°$, and $\gamma_2 = 54.75°$ for the second site. Substituting the values of α and β into

eqs. [5]–[10], we get:

$$[11]\quad V_i(\gamma_i) = \begin{bmatrix} \sin^2\gamma_i V_{YY} + \cos^2\gamma_i V_{ZZ} & \sin\gamma_i \cos\gamma_i (V_{YY} - V_{ZZ}) & 0 \\ \sin\gamma_i \cos\gamma_i (V_{YY} - V_{ZZ}) & \cos^2\gamma_i V_{YY} + \sin^2\gamma_i V_{ZZ} & 0 \\ 0 & 0 & V_{XX} \end{bmatrix}$$

Let the populations of the two sites equal P_1 and P_2. The weighted average of $V_i(\gamma_i)$ is given by:

$$[12]\quad \overline{V(\gamma)} = \begin{bmatrix} \sin^2\gamma V_{YY} + \cos^2\gamma V_{ZZ} & \sin\gamma\cos\gamma (V_{YY} - V_{ZZ})(P_2 - P_1) & 0 \\ \sin\gamma\cos\gamma (V_{YY} - V_{ZZ})(P_2 - P_1) & \cos^2\gamma V_{YY} + \sin^2\gamma V_{ZZ} & 0 \\ 0 & 0 & V_{XX} \end{bmatrix}$$

The eigenvalues, λ_i can be obtained by diagonalization.

$$[13]\quad \lambda_1 = \frac{(V_{YY} + V_{ZZ}) + (V_{YY} - V_{ZZ})\sqrt{1 - 4\sin^2\gamma\cos^2\gamma(1 - (P_2 - P_1)^2)}}{2}$$

$$\lambda_2 = \frac{(V_{YY} + V_{ZZ}) + (V_{YY} - V_{ZZ})\sqrt{1 - 4\sin^2\gamma\cos^2\gamma(1 - (P_2 - P_1)^2)}}{2}$$

$$\lambda_3 = V_{XX}$$

We can express the components of the unaveraged electric field gradient tensor, V_{ii}, in terms of χ and η then set γ to one half of the tetrahedral angle. The frequency splittings, $\Delta\nu'_{XX}$, $\Delta\nu'_{YY}$, and $\Delta\nu'_{ZZ}$ in the averaged spectrum can then be expressed as follows:

$$[14]\quad -\Delta\nu'_{XX} = \frac{\chi}{8}(3(1-\eta) - (3+\eta)\sqrt{1 + 8(P_2 - P_1)^2})$$

$$[15]\quad -\Delta\nu'_{YY} = -\frac{3}{4}\chi(1-\eta)$$

$$[16]\quad \Delta\nu'_{ZZ} = \frac{\chi}{8}(3(1-\eta) + (3+\eta)\sqrt{1 + 8(P_2 - P_1)^2})$$

If we know the quadrupolar coupling constant and asymmetry parameter for the rigid spectrum and have measured the splittings in an averaged spectrum, we can directly evaluate the populations of the sites at a given temperature. Unfortunately, χ and η are not available in the literature and our equipment did not allow the measurement of spectra at sufficiently low temperatures for their experimental determination. However, these data have been reported for cyclohexane (20) ($\chi = 173.7 \pm 1.7$ kHz and $\eta \leq 0.01$). If we assume that these parameters are not significantly different for our case, we can take $\chi = 174$ kHz and $\eta = 0$ and obtain the populations from eqs. [14] and [16]. The ratio of populations is expected to follow the Boltzman distribution, hence a plot of $\ln(P_1/P_2)$ vs. $1/T$ should be linear with slope $-\Delta E/R$, where ΔE is the energy difference between the two conformations and R is the gas constant. These data are plotted in Fig. 6*A* and the energy difference obtained is 3.2 ± 0.3 kJ/mol.

^{2}H T_1 relaxation times were measured as a function of temperature. When dominated by the quadrupolar interaction, in the case of a two-site exchange, the rate of relaxation can be described by (21):

$$[17]\quad \frac{1}{T_1} = \frac{3}{16}\chi^2\left(\frac{\tau_c}{1 + (\omega_0\tau_c)^2} + \frac{4\tau_c}{1 + (2\omega_0\tau_c)^2}\right)$$

Fig. 6. (*A*) Plot of the population ratios calculated from eqs. [14] and [16] for **6b** as a function of temperature. (*B*) Same as *A* for **5b**.

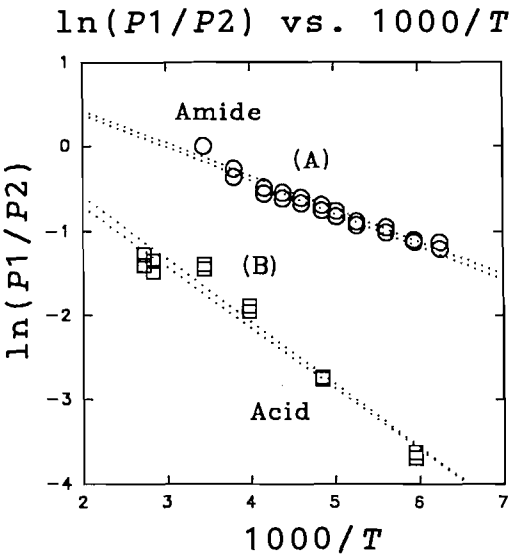

where ω_0 is the angular Larmor frequency and τ_c is the correlation time. The T_1's were calculated from the inner singularities of the powder spectra. A plot of log T_1 vs. reciprocal temperature is presented in Fig. 7. A T_1 minimum is observed at ~196 K. This minimum occurs when $\omega_0\tau_c = 0.6158$ and can be used to determine the correlation time at the temperature of the minimum. The correlation time at 196 K is 3.19 ns. The slope of the line in the high-temperature regime can be used to evaluate an activation barrier from the Arrhenius relation. The activation barrier was evaluated at 12.3 ± 0.2 kJ/mol. We can compare this to that measured for cyclohexene in solution (22.2 kJ/mol) (22). Strictly speaking, activation energies and correlation times evaluated in this way assume that the populations remain equal throughout the entire temperature range, therefore the activation barrier

Fig. 7. Plot of $\ln(T_1)$ vs. $(1000/T)$ for the ^2H data collected for **6b**.

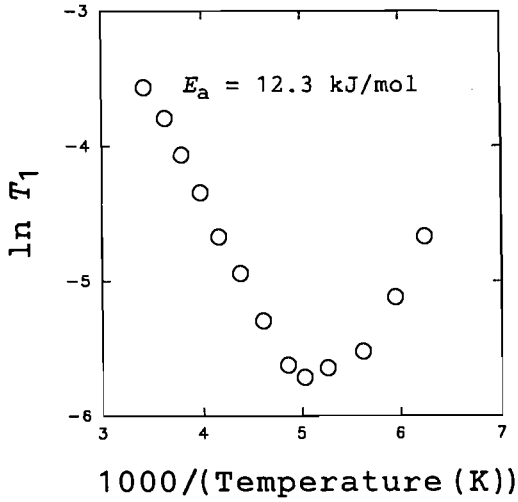

and correlation time presented here are best referred to as "apparent." The relatively low "apparent" activation energy evaluated here may be due to the large amount of void space in the vicinity of the cyclohexene moiety of **6b** in the crystal lattice.

If we make the reasonable assumption that **6b** is structurally identical to **6a**, we can conclude that the disorder observed in the X-ray diffraction data is dynamic in nature. By extrapolation of the data in Fig. 6*B* we can estimate the populations of the two conformations to be approximately 86:14. Based on this information, the initial 0.75:0.25 population ratio used in the X-ray diffraction data was replaced by 86:14 and a further refinement carried out. This modification, however, made very little difference to the atomic coordinates or thermal parameters.

The solid state ^{13}C CP/MAS NMR spectrum of **5a** taken at room temperature is shown in Fig. 8*A* with the corresponding dipolar dephased spectrum in Fig. 8*B*. Unlike the ^{13}C CP/MAS dipolar dephased spectrum of **6a**, the spectrum of **5a** does not show any significant intensity for the methylene carbons in the 6 and 7 positions. This observation can mean one of two things. Either the system is rigid with one or more conformations or there is a similar conformational exchange as observed for **6a** except that the population difference is very close to unity. In either case the net $^{13}C - ^1H$ dipolar interaction would still be large and the ^{13}C signal for the methylenes would be expected to decay significantly during the 40 μs dipolar dephasing delay.

The wideline solid state ^2H NMR spectra of **5b** are given in Fig. 9 as a function of temperature. As with **6b**, the spectra are narrower than expected for a completely rigid system. Also similar to the ^2H spectra of **6b**, the spectra are temperature dependent and in the fast-motion limit. This eliminates the hypothesis that the system is completely rigid. A plot of the spectral frequency separations as a function of temperature are given in Fig. 10. The data are very similar to those in Fig. 4, indicating that the motion is of the same type as that observed for **6b**. If we assume the same model for dynamic disorder as in **6b** and that the quadrupolar coupling constant for the rigid system is 174 kHz with $\eta = 0$, then the

Fig. 8. (*A*) ^{13}C CP/MAS NMR spectrum of **5a** at room temperature. (*B*) Same as *A* with a 40 μs dipolar dephasing delay. The peaks marked with an asterisk are spinning side bands.

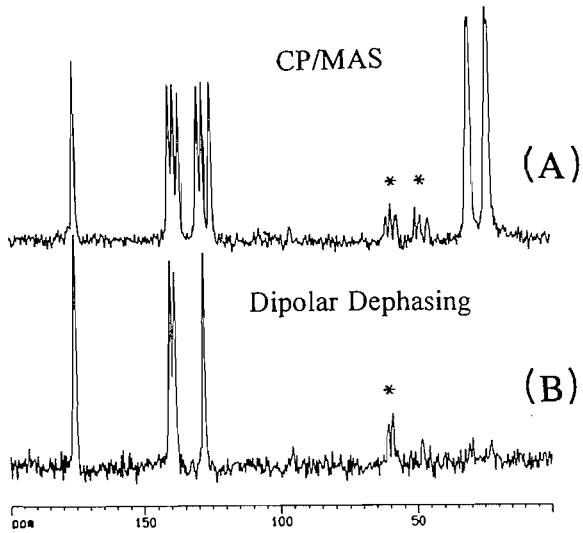

Fig. 9. Broadline solid state ^2H NMR spectra of **5b** recorded as a function of temperature. The relaxation delay was 10 s.

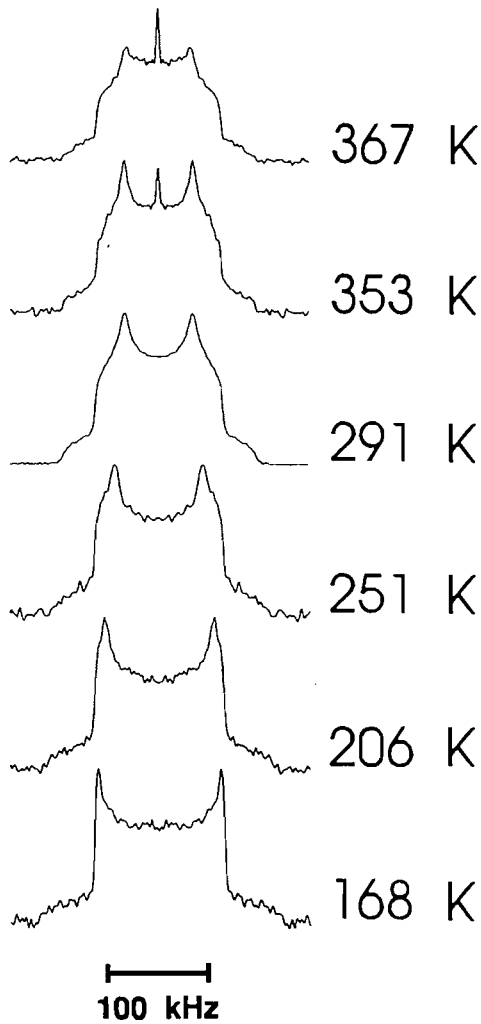

Fig. 10. Plot of the frequency differences, $\Delta\nu'_{XX}$, $\Delta\nu'_{YY}$, and $\Delta\nu'_{ZZ}$, between the features of the solid state ^2H spectra of **5b** as a function of temperature.

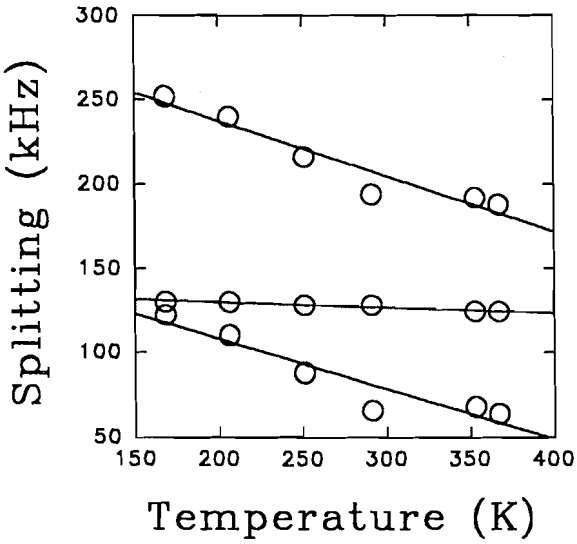

populations can be calculated as before and the energy difference between the two conformations evaluated. The data are plotted in Fig. 6*B* and give $\Delta E = 6.1 \pm 0.2$ kJ/mol. From both the ^{13}C and ^2H solid state NMR data it is apparent that **5b** undergoes an exchange akin to a chair-to-chair inversion of the cyclohexene ring in the solid state where one of the conformations is highly favoured with respect to the other. The fact that the population difference for **5b** is larger than that for **6b** may suggest that for the case of the acid there is less void space around the cyclohexene ring in the crystal lattice.

Conclusion

The X-ray crystal structure obtained for **6a** shows a molecular conformation where the carbonyl bond is almost normal to the plane of the aromatic ring. This conformation leaves a great deal of void space around the cyclohexene moiety, giving it the freedom to undergo molecular motions. The crystal structure shows that there are two distinct conformations present but is unable to confirm whether they are disordered statically or dynamically. Solid state ^{13}C CP/MAS data taken at room temperature reveal that the disorder is dynamic at room temperature, and the ^2H NMR data are able to evaluate the population ratios as a function of temperature as well as determine an apparent activation barrier based on a simple two-site ring inversion. The ^2H NMR data for **5b** support the notion that the same sort of ring inversion occurs in this compound; however, the population differences are much larger. The large population difference is consistent with the absence of methylene signals in the ^{13}C CP/MAS spectrum with dipolar dephasing.

References

1. M. Mehring. *In* NMR basic priciples and progress: High-resolution NMR spectroscopy of solids. *Edited by* P. Diehl, E. Fluck, and R. Kosfeld. Springer-Verlag, New York. 1976.
2. A. Abragam. *In* The principles of nuclear magnetism. *Edited by* R.K. Adair, R.J. Elliot, W.C. Marshal, and D.H. Wilkinson. Clarendon Press, Oxford. 1961. pp. 424–479.
3. K. Beshah and R.G. Griffin. J. Magn. Reson. **84**, 268 (1989).
4. K. Beshah, E.T. Olejniczak, and R.G. Griffin. J. Chem. Phys. **88**, 4730 (1987).
5. M.J. Collins, C.I. Ratcliffe, and J.A. Ripmeester. J. Phys. Chem. **93**, 7495 (1987).
6. E. Meirovitch and J.H. Freed. Chem. Phys. Lett. **64**, 311 (1979).
7. A.J. Vega and Z. Luz. J. Chem. Phys. **86**, 1803 (1986).
8. R.J. Wittebort, E.T. Olejniczak, and R.G. Griffin. J. Chem. Phys. **86**, 5411 (1987).
9. M.S. Greenfield, A.D. Ronemus, R.L. Vold, R.R. Vold, P.D. Ellis, and T.E. Raidy. J. Magn. Reson. **72**, 89 (1987).
10. H.W. Spiess and H.J. Sillescu. J. Magn. Reson. **42**, 381 (1981).
11. J.A. Ripmeester. J. Chem. Phys. **85**, 747 (1986).
12. M.A. Hemminga and P.A. de Jager. J. Magn. Reson. **51**, 339 (1983).
13. J.H. Davis, K.R. Jeffrey, M. Bloom, M.I. Valic, and T.P. Higgs. Chem. Phys. Lett. **42**, 390 (1976).
14. Terrence J. Connolly. Ph.D. Thesis, University of Ottawa (1996).
15. R.K. Harris and A.C. Olivieri. Prog. NMR Spectrosc. **24**, 435 (1992).
16. C.A. McDowell, A. Naito, J.R. Scheffer, and Y-F Wong. Tetrahedron Lett. **22**, 4779 (1981).
17. L.B. Alemany, D.M. Grant, T.D. Alger, and R.J. Pugmire. J. Am. Chem. Soc. **105**, 6697 (1983).
18. R.G. Barnes. Adv. Nucl. Quadrupole Reson. **1**, 335 (1974).
19. J. Mathews and R.L. Walker. *In* Mathematical methods of physics. W.A. Benjamin, New York. 1965. p. 374.
20. R.G. Barnes and J.W. Bloom. J. Chem. Phys. **56**, 1549 (1972).
21. D.A. Torchia and A. Szabo. J. Magn. Reson. **49**, 107 (1982).
22. F.A.L. Anet and M.Z. Haq. J. Am. Chem. Soc. **87**, 3147 (1965).